Penerbit Akademia Baru

CFD Letters

Journal homepage: www.akademiabaru.com/cfdl.html
ISSN: 2180-1363

Analytical and Numerical Solutions to the 2D Sakiadis Flow of Casson Fluid with Cross Diffusion, Inclined Magnetic Force, Viscous Dissipation and Thermal Radiation Based on Buongiorno's Mathematical Model

Open Access

Emran Khoshrouye Ghiasi[1], Reza Saleh[1,*]

[1] Department of Mechanical Engineering, College of Engineering, Mashhad Branch, Islamic Azad University, Mashhad, Iran

ARTICLE INFO

Article history:
Received 3 December 2018
Received in revised form 20 December 2018
Accepted 10 January 2019
Available online 11 January 2019

Keywords:
Sakiadis flow, Nanoparticle, Buongiorno's mathematical model, HAM, RKF45M

ABSTRACT

In this paper, the homotopy analysis method (HAM) and Runge-Kutta-Fehlberg fourth-fifth order method (RKF45M) are applied to investigate the 2D Sakiadis flow of non-Newtonian Casson fluid with convective boundary conditions based on the Buongiorno's mathematical model. The governing boundary layer equations of continuity, momentum, thermal energy and nanoparticle concentration are derived and converted to the dimensionless form via the similarity variables. The present solutions agree entirely with those available results in the literatures. A parametric study is also performed to illustrate the effects of pertinent parameters on the fluid flow. It is shown that the skin friction coefficient for a non-Newtonian fluid is found to be higher than that of the Newtonian one. Furthermore, the thermal boundary layer thickness is greatly affected by the resistive Lorentz force and viscous dissipation.

1. Introduction

In fluid mechanics the Sakiadis problem [1,2] which can be considered as a variant of the well-known Blasius equation [3], is concerned with the boundary layer flow in a quiescent fluid. The most important aspect of this problem is to provide the fluid motion by a moving flat plate. In recent years, there has been an increase in the number of research studies dealt with this problem. In this regard, Sulochana *et al.,* [4] analyzed the magnetohydrodynamic (MHD) axisymmetric Sakiadis flow of Cu-H_2O and $Al_{50}Cu_{50}$-H_2O nanofluids past a thin horizontal needle considering the Joule heating. They developed those reported by Soid *et al.,* [5] and showed that accounting for the effect of Lorentz force increases the thermal boundary layer thickness. They also found that the relative velocity of $Al_{50}Cu_{50}$-H_2O nanofluid is greater in the vicinity of the wall, compared to the Cu-

* *Corresponding author.*
E-mail address: R-Saleh@mshdiau.ac.ir (Reza Saleh)

H_2O nanofluid. Cortell Bataller [6] investigated the effects of convective heat transfer with thermal radiation on the Blasius and Sakiadis flow numerically through the Runge-Kutta fourth-order method (RK4M). They found that the Sakiadis flow yields a thicker thermal boundary layer than the Blasius flow at low Prandtl numbers. They also reported the significant effect of thermal diffusion on the wall temperature. Finally, they concluded that their findings are in agreement with those of Aziz [7]. Hayat *et al.,* [8] performed heat transfer analysis in the Blasius and Sakiadis flow of an Eyring-Powell fluid with the constant heat flux and convective boundary conditions, and found that the thermal boundary layer thickness decreases with an increase in the Prandtl number. They also illustrated importance of the external convection resistance inside the surface. Bachok *et al.,* [9] optimized the Blasius and Sakiadis flow of Cu-H_2O, Al_2O_3-H_2O and TiO_2-H_2O nanofluids presented by Ahmad *et al.,* [10] and showed that Cu-H_2O and TiO_2-H_2O nanofluids take the lowest and highest heat transfer rates, respectively. They also emphasized that in case of zero heat flux, their findings are fully consistent with those of Ishak *et al.,* [11]. Pantokratoras [12] studied the Blasius and Sakiadis flow of a Carreau fluid numerically through the finite difference method (FDM). He showed that the momentum boundary layer thickness decreases with an increase in the Deborah number. He also investigated effects of the Deborah number on the shear-thinning and Shear-thickening fluids (see Ref. [13]) for both the Blasius and Sakiadis flow cases. Hayat *et al.,* [14] analyzed the combined effects of convective heat transfer and viscous dissipation on the Blasius and Sakiadis flow of an upper-converted Maxwell (UCM) fluid using the HAM, and indicated that the heat transfer rates decreases with an increase in the Eckert number. They also found that the thermal boundary layer thickness is significantly affected by the Biot number. With mathematical precision, Girgin [15] employed the generalized iterative differential quadrature method (GIDQM) to investigate the effects of variable fluid properties on the Blasius and Sakiadis flow, and showed that his findings are consistent with those provided by Arikoglu and Ozkol [16] and Andersson and Aarseth [17]. Xu and Guo [18] developed a fixed point iterative method (FPIM) for solving the Blasius and Sakiadis flow in terms of a series of linear differential equations. Fazio [19] proved that the iterative transformation method (ITM) is applicable to the Sakiadis flow. He also emphasized that the skin friction coefficient in this case is 1.34 times greater than that of the Blasius flow (see Ref. [20]). It should be emphasized here that more details can be found in Refs. [21-30].

Motivated by the aforementioned research studies, this paper provides analytical and numerical solutions for dealing with the heat and mass transfer analysis in the Sakiadis flow of Casson fluid with convective boundary conditions. The Buongiorno's mathematical model [31] related to the Brownian motion and thermophoresis effects has also been utilized to simulate slip mechanisms in the nanoparticles. The organization of this paper is as follows.

Section 2 provides a very detailed description of the governing equations and its non-dimensionalization. Section 3 states the analytical and numerical solution methods. The results and discussion are reported in section 4. The concluding remarks are summarized in section 5.

2. Governing Equations

The non-Newtonian fluids are categorized into three main types: Time-independent, time-dependent and viscoelastic fluids [32, 33]. In the case of time-dependent fluids, the viscosity is not dependent on the duration of shearing [34]. In this section, one may define the time-independent Casson fluid [35] which has the following constitutive equation

$$\mu\dot{\gamma} = \begin{cases} \left(1 - \sqrt{\frac{\bar{\tau}_0}{|\bar{\tau}|}}\right)^2 \bar{\tau}, |\bar{\tau}| > \bar{\tau}_0, \\ 0, |\bar{\tau}| \leq \bar{\tau}_0, \end{cases} \tag{1}$$

where μ is the plastic dynamic viscosity, $\dot{\gamma}$ is the rate of shear strain, $\bar{\tau}_0$ is the yield stress, $\bar{\tau}$ is the Cauchy stress tensor and $|\bar{\tau}|$ is the magnitude of $\bar{\tau}$. From Eq. 1, it is apparent that the viscosity decreases with an increase in the rate of shear strain. Moreover, if the yield stress is equal to zero, the Casson fluid reduces to the Newtonian type [34].

For a 2D flow in the Cartesian coordinate system, the velocity, temperature and nanoparticle concentration fields are stated as

$$\mathbf{V} = [u(x,y), v(x,y)], \mathbf{T} = T(x,y), \mathbf{C} = C(x,y), \tag{2}$$

where u and v are the velocity components along the x- and y-axes, respectively, T is the temperature and C is the nanoparticle concentration.

Using the above-mentioned assumptions, the governing boundary layer equations of continuity, momentum, thermal energy and nanoparticle concentration can be written as follows

$$\begin{cases} \frac{\partial u}{\partial x} + \frac{\partial v}{\partial y} = 0, \\ u\frac{\partial u}{\partial x} + v\frac{\partial u}{\partial y} = \upsilon\left(1 + \frac{1}{\lambda}\right)\frac{\partial^2 u}{\partial y^2} - \frac{\sigma B_0^2}{\rho_f} u \sin^2\psi, \\ u\frac{\partial T}{\partial x} + v\frac{\partial T}{\partial y} = \alpha\frac{\partial^2 T}{\partial y^2} + \frac{\upsilon}{c_p}\left(1 + \frac{1}{\lambda}\right)\left(\frac{\partial u}{\partial y}\right)^2 + \zeta\left[D_{\mathrm{B}}\frac{\partial C}{\partial y}\frac{\partial T}{\partial y} + \frac{D_{\mathrm{T}}}{T_\infty}\left(\frac{\partial T}{\partial y}\right)^2\right] - \frac{1}{\rho_f c_p}\frac{\partial q_r}{\partial y}, \\ u\frac{\partial C}{\partial x} + v\frac{\partial C}{\partial y} = D_{\mathrm{B}}\frac{\partial^2 C}{\partial y^2} + \frac{D_{\mathrm{T}}}{T_\infty}\frac{\partial^2 T}{\partial y^2}, \end{cases} \tag{3}$$

along with the following boundary conditions

$$\begin{cases} \text{at } y = 0: u = U_w, v = 0, T = T_w, C = C_w, \\ \text{as } y \to \infty: u \to 0, T \to T_\infty, C \to C_\infty, \end{cases} \tag{4}$$

where υ is the kinematic viscosity, λ is the Casson fluid parameter, σ is the electrical conductivity, B_0 is the magnetic field strength, ρ_f is the fluid density, ψ is the inclination angle of the magnetic field, α is the thermal diffusivity, c_p is the specific heat of the fluid at constant pressure, $\zeta = \frac{(\rho c)_p}{(\rho c)_f}$ is the ratio of nanoparticle heat capacity to the base fluid heat capacity, D_{B} is the Brownian diffusion coefficient, D_{T} is the thermophoresis diffusion coefficient, T_∞ is the ambient temperature, q_r is the radiation heat flux, U_w is the constant velocity of the moving flat plate, T_w is the wall temperature, C_w is the nanoparticle concentration around the wall and C_∞ is the ambient nanoparticle concentration.

According to the Rosseland approximation [36] the radiation heat flux involved in Eq. 3 may be expressed in the following form

$$q_r = -\frac{4\sigma_{SB}}{3\beta_R}\frac{\partial T^4}{\partial y}, \tag{5}$$

where σ_{SB} and β_R are the Stefan-Boltzmann constant and Rosseland mean absorption coefficient, respectively.

It is to be noted that the fluid-phase temperature difference within the flow is almost negligible and hence T^4 can be expanded into a Taylor series with respect to T_∞ as $T^4 \cong 4TT_\infty^3 - 3T_\infty^4$. Then, the radiation heat flux results in $q_r = -\frac{16T_\infty^3\sigma_{SB}}{3\beta_R}\frac{\partial T}{\partial y}$.

To convert above equations to the dimensionless form, the following variables can be expressed

$$\psi = \sqrt{U_w \nu x} f(\eta), \eta = y\sqrt{\frac{U_w}{\nu x}}, \theta(\eta) = \frac{T-T_\infty}{T_w-T_\infty}, \phi(\eta) = \frac{C-C_\infty}{C_w-C_\infty}, \tag{6}$$

where ψ is the stream function which is governed by $u = \frac{\partial \psi}{\partial y}$ and $v = -\frac{\partial \psi}{\partial x}$, f is the similarity function, η is the similarity parameter, θ is the dimensionless temperature and ϕ is the dimensionless nanoparticle concentration.

Substituting Eq. 6 into Eq. 3 and Eq. 4 gives

$$\begin{cases} \left(1+\frac{1}{\lambda}\right)\frac{\partial^3 f}{\partial \eta^3} + f\frac{\partial^2 f}{\partial \eta^2} - \frac{\partial f}{\partial \eta}\left(\frac{\partial f}{\partial \eta} + \mathrm{Ha}^2 \sin^2 \psi\right) = 0, \\ \frac{1}{\mathrm{Pr}}\frac{\partial^2 \theta}{\partial \eta^2} + \frac{1}{2} f\frac{\partial \theta}{\partial \eta} + \mathrm{Nb}\frac{\partial \phi}{\partial \eta}\frac{\partial \theta}{\partial \eta} + \mathrm{Nt}\left(\frac{\partial \theta}{\partial \eta}\right)^2 + \frac{1}{2}\mathrm{Nr} f\frac{\partial \theta}{\partial \eta} + \mathrm{Ec}\left(1+\frac{1}{\lambda}\right)\left(\frac{\partial^2 f}{\partial \eta^2}\right)^2 = 0, \\ \frac{\partial^2 \phi}{\partial \eta^2} + \frac{1}{2}\mathrm{Le} f\frac{\partial \phi}{\partial \eta} + \frac{\mathrm{Nt}}{\mathrm{Nb}}\frac{\partial^2 \theta}{\partial \eta^2} = 0, \end{cases} \tag{7}$$

and,

$$\begin{cases} \text{at } \eta = 0: f = 0, \frac{\partial f}{\partial \eta} = 1, \theta = 1, \phi = 1, \\ \text{as } \eta \to \infty: \frac{\partial f}{\partial \eta} \to 0, \theta \to 0, \phi \to 0, \end{cases} \tag{8}$$

where $\mathrm{Ha}^2 = \frac{\sigma B_0^2}{\rho U_w}$ is the square of the Hartmann number, $\mathrm{Pr} = \frac{\upsilon}{\alpha}$ is the Prandtl number, $\mathrm{Nb} = \frac{\zeta D_\mathrm{B}}{\upsilon}(C_w - C_\infty)$ is the Brownian motion parameter, $\mathrm{Nt} = \frac{\zeta D_\mathrm{T}}{\upsilon T_\infty}(T_w - T_\infty)$ is the thermophoresis parameter, $\mathrm{Nr} = \frac{k\beta_R}{4\sigma_{SB}T_\infty^3}$ is the radiation parameter, $\mathrm{Ec} = \frac{U_w^2}{c_p(T_w-T_\infty)}$ is the Eckert number and $\mathrm{Le} = \frac{\alpha}{D_\mathrm{B}}$ is the Lewis number.

The skin friction coefficient, local Nusselt number and local Sherwood number are defined as

$$\mathrm{C}_f = 2\frac{\tau_w}{\rho U_w^2}, \mathrm{Nu}_x = \frac{x q_w}{k(T_w-T_\infty)}, \mathrm{Sh}_x = \frac{x q_m}{D_\mathrm{B}(C_w-C_\infty)}, \tag{9}$$

where,

$$\tau_w = \mu\left(1+\frac{1}{\lambda}\right)\left(\frac{\partial u}{\partial y}\right)_{y=0}, q_w = -k\left(\frac{\partial T}{\partial y}\right)_{y=0}, q_m = -D_\mathrm{B}\left(\frac{\partial C}{\partial y}\right)_{y=0}. \tag{10}$$

Substituting Eq. 6 and Eq. 10 into Eq. 9 gives

$$\mathrm{C}_f\mathrm{Re}_x^{\frac{1}{2}} = \left(1+\frac{1}{\lambda}\right)\left(\frac{\partial^2 f}{\partial \eta^2}\right)_{\eta=0}, \mathrm{Nu}_x\mathrm{Re}_x^{-\frac{1}{2}} = -\left(\frac{\partial \theta}{\partial \eta}\right)_{\eta=0}, \mathrm{Sh}_x\mathrm{Re}_x^{-\frac{1}{2}} = -\left(\frac{\partial \phi}{\partial \eta}\right)_{\eta=0}, \tag{11}$$

where $\mathrm{Re}_x = \frac{xU_w}{\upsilon}$ is the local Reynolds number based on the wall velocity.

The following section contains the analytical and numerical solutions for Eq. 7 and Eq. 8 that may be amenable to the nonlinear boundary value problems.

3. Solution method

3.1 HAM

Let us choose the appropriate initial guesses as follows

$$f_0(\eta) = 1 - \exp(-\eta), \theta_0(\eta) = \exp(-\eta), \phi_0(\eta) = \exp(-\eta). \tag{12}$$

The auxiliary linear operators can be expressed as

$$\mathbf{L}_f \equiv \frac{\partial^3 f}{\partial \eta^3} - \frac{\partial f}{\partial \eta}, \mathbf{L}_\theta \equiv \frac{\partial^2 \theta}{\partial \eta^2} - \theta, \mathbf{L}_\phi \equiv \frac{\partial^2 \phi}{\partial \eta^2} - \phi, \tag{13}$$

which have the following properties

$$\begin{cases} \mathbf{L}_f[c_1 + c_2\exp(\eta) + c_3\exp(-\eta)] = 0, \\ \mathbf{L}_\theta[c_4\exp(\eta) + c_5\exp(-\eta)] = 0, \\ \mathbf{L}_\phi[c_6\exp(\eta) + c_7\exp(-\eta)] = 0, \end{cases} \tag{14}$$

where $c_1, c_2, \ldots, c_7$ are the arbitrary constants. The zeroth-order problems correspond to Eq. 7 and Eq. 8 are constructed in the following forms

$$\begin{cases} (1-p)\mathbf{L}_f\left[\hat{f}(\eta,p) - f_0(\eta)\right] = ph_f\mathbf{N}_f\left[\hat{f}(\eta,p)\right], \\ (1-p)\mathbf{L}_\theta\left[\hat{\theta}(\eta,p) - \theta_0(\eta)\right] = ph_\theta\mathbf{N}_\theta\left[\hat{f}(\eta,p), \hat{\theta}(\eta,p), \hat{\phi}(\eta,p)\right], \\ (1-p)\mathbf{L}_\phi\left[\hat{\phi}(\eta,p) - \phi_0(\eta)\right] = ph_\phi\mathbf{N}_\phi\left[\hat{f}(\eta,p), \hat{\theta}(\eta,p), \hat{\phi}(\eta,p)\right], \end{cases} \tag{15}$$

and,

$$\begin{cases} \text{at } \eta = 0\text{: } \hat{f}(\eta,p) = 0, \frac{\partial \hat{f}(\eta,p)}{\partial \eta} = 1, \hat{\theta}(\eta,p) = 1, \hat{\phi}(\eta,p) = 1, \\ \text{as } \eta \to \infty\text{: } \frac{\partial \hat{f}(\eta,p)}{\partial \eta} \to 0, \hat{\theta}(\eta,p) \to 0, \hat{\phi}(\eta,p) \to 0, \end{cases} \tag{16}$$

where $0 \le p \le 1$ is an embedding parameter, h_f, h_θ and h_ϕ are the non-zero auxiliary parameters, and $\mathbf{N}_f$, $\mathbf{N}_\theta$ and $\mathbf{N}_\phi$ are the nonlinear operators which can be defined as follows

$$\begin{cases} \mathbf{N}_f\left[\hat{f}(\eta,p)\right] = \left(1+\frac{1}{\lambda}\right)\frac{\partial^3 \hat{f}}{\partial \eta^3} + \hat{f}\frac{\partial^2 \hat{f}}{\partial \eta^2} - \frac{\partial \hat{f}}{\partial \eta}\left(\frac{\partial \hat{f}}{\partial \eta} + \mathrm{Ha}^2 \sin^2 \psi\right), \\ \mathbf{N}_\theta\left[\hat{f}(\eta,p), \hat{\theta}(\eta,p), \hat{\phi}(\eta,p)\right] = \frac{1}{\mathrm{Pr}}\frac{\partial^2 \hat{\theta}}{\partial \eta^2} + \frac{1}{2}\hat{f}\frac{\partial \hat{\theta}}{\partial \eta} + \mathrm{Nb}\frac{\partial \hat{\phi}}{\partial \eta}\frac{\partial \hat{\theta}}{\partial \eta} + \mathrm{Nt}\left(\frac{\partial \hat{\theta}}{\partial \eta}\right)^2 \\ \quad + \frac{1}{2}\mathrm{Nr}\hat{f}\frac{\partial \hat{\theta}}{\partial \eta} + \mathrm{Ec}\left(1+\frac{1}{\lambda}\right)\left(\frac{\partial^2 \hat{f}}{\partial \eta^2}\right)^2, \\ \mathbf{N}_\phi\left[\hat{f}(\eta,p), \hat{\theta}(\eta,p), \hat{\phi}(\eta,p)\right] = \frac{\partial^2 \hat{\phi}}{\partial \eta^2} + \frac{1}{2}\mathrm{Le}\hat{f}\frac{\partial \hat{\phi}}{\partial \eta} + \frac{\mathrm{Nt}}{\mathrm{Nb}}\frac{\partial^2 \hat{\theta}}{\partial \eta^2}. \end{cases} \tag{17}$$

When $p = 0$, Eq. 5 converts to

$$\mathbf{L}_f\left[\hat{f}(\eta,0) - f_0(\eta)\right] = 0, \mathbf{L}_\theta\left[\hat{\theta}(\eta,0) - \theta_0(\eta)\right] = 0, \mathbf{L}_\phi\left[\hat{\phi}(\eta,0) - \phi_0(\eta)\right] = 0, \tag{18}$$

and when $p = 1$, Eq. 5 converts to

$$\begin{cases} \mathbf{N}_f\left[\hat{f}(\eta,1)\right] = 0, \\ \mathbf{N}_\theta\left[\hat{f}(\eta,1), \hat{\theta}(\eta,1), \hat{\phi}(\eta,1)\right] = 0, \\ \mathbf{N}_\phi\left[\hat{f}(\eta,1), \hat{\theta}(\eta,1), \hat{\phi}(\eta,1)\right] = 0. \end{cases} \tag{19}$$

expanding $\hat{f}(\eta,p)$, $\hat{\theta}(\eta,p)$ and $\hat{\phi}(\eta,p)$ into the Taylor series with respect to p gives

$$\begin{cases} \hat{f}(\eta,p) = f_0(p) + \sum_{m=1}^{\infty} f_m(\eta)p^m, \\ \hat{\theta}(\eta,p) = \theta_0(p) + \sum_{m=1}^{\infty} \theta_m(\eta)p^m, \\ \hat{\phi}(\eta,p) = \phi_0(p) + \sum_{m=1}^{\infty} \phi_m(\eta)p^m, \end{cases} \tag{20}$$

where,

$$\begin{cases} f_m(\eta) = \left(\frac{1}{m!}\frac{\partial^m \hat{f}(\eta,p)}{\partial p^m}\right)_{p=0}, \\ \theta_m(\eta) = \left(\frac{1}{m!}\frac{\partial^m \hat{\theta}(\eta,p)}{\partial p^m}\right)_{p=0}, \\ \phi_m(\eta) = \left(\frac{1}{m!}\frac{\partial^m \hat{\phi}(\eta,p)}{\partial p^m}\right)_{p=0}. \end{cases} \tag{21}$$

If the initial guesses, auxiliary linear operators and auxiliary parameters are properly chosen, Eq. 20 converges at $p = 1$ as follows

$$\begin{cases} f(\eta) = \sum_{m=0}^{\infty} f_m(\eta), \\ \theta(\eta) = \sum_{m=0}^{\infty} \theta_m(\eta), \\ \phi(\eta) = \sum_{m=0}^{\infty} \phi_m(\eta). \end{cases} \tag{22}$$

Differentiating Eq. 15 m times with respect to p, setting $p = 0$ and dividing them by $m!$ gives the following mth-order problems

$$\begin{cases} \mathbf{L}_f[f_m(\eta) - \chi_m f_{m-1}(\eta)] = h_f \mathbf{R}_m^f(\eta), \\ \mathbf{L}_\theta[\theta_m(\eta) - \chi_m \theta_{m-1}(\eta)] = h_\theta \mathbf{R}_m^\theta(\eta), \\ \mathbf{L}_\phi[\phi_m(\eta) - \chi_m \phi_{m-1}(\eta)] = h_\phi \mathbf{R}_m^\phi(\eta), \end{cases} \tag{23}$$

and,

$$\begin{cases} \text{at } \eta = 0\text{: } f(\eta) = 0, \frac{\partial f(\eta)}{\partial \eta} = 0, \theta(\eta) = 0, \phi(\eta) = 0, \\ \text{as } \eta \to \infty\text{: } \frac{\partial f(\eta)}{\partial \eta} \to 0, \theta(\eta) \to 0, \phi(\eta) \to 0, \end{cases} \tag{24}$$

where χ_m and $\mathbf{R}_m^f$, $\mathbf{R}_m^\theta$ and $\mathbf{R}_m^\phi$ can be written as

$$\chi_m = \begin{cases} 0, m \le 1, \\ 1, m > 1, \end{cases} \tag{25}$$

$$\begin{cases} \mathbf{R}_m^f(\eta) = \left(1 + \frac{1}{\lambda}\right) \frac{\partial^3 f_{m-1}}{\partial \eta^3} + \sum_{n=0}^{m-1} f_n \frac{\partial^2 f_{m-n-1}}{\partial \eta^2} - \sum_{n=0}^{m-1} \frac{\partial f_n}{\partial \eta} \frac{\partial f_{m-n-1}}{\partial \eta} \\ -\mathrm{Ha}^2 \sin^2 \psi \frac{\partial f_{m-1}}{\partial \eta}, \\ \mathbf{R}_m^\theta(\eta) = \frac{1}{\mathrm{Pr}} \frac{\partial^2 \theta_{m-1}}{\partial \eta^2} + \frac{1}{2} \sum_{n=0}^{m-1} f_n \frac{\partial \theta_{m-n-1}}{\partial \eta} + \mathrm{Nb} \sum_{n=0}^{m-1} \frac{\partial \phi_n}{\partial \eta} \frac{\partial \theta_{m-n-1}}{\partial \eta} \\ +\mathrm{Nt} \sum_{n=0}^{m-1} \frac{\partial \theta_n}{\partial \eta} \frac{\partial \theta_{m-n-1}}{\partial \eta} + \frac{1}{2} \mathrm{Nr} \sum_{n=0}^{m-1} f_n \frac{\partial \theta_{m-n-1}}{\partial \eta} + \mathrm{Ec} \left(1 + \frac{1}{\lambda}\right) \sum_{n=0}^{m-1} \frac{\partial^2 f_n}{\partial \eta^2} \frac{\partial^2 f_{m-n-1}}{\partial \eta^2}, \\ \mathbf{R}_m^\phi(\eta) = \frac{\partial^2 \phi_{m-1}}{\partial \eta^2} + \frac{1}{2} \mathrm{Le} \sum_{n=0}^{m-1} f_n \frac{\partial \phi_{m-n-1}}{\partial \eta} + \frac{\mathrm{Nt}}{\mathrm{Nb}} \frac{\partial^2 \theta_{m-1}}{\partial \eta^2}. \end{cases} \tag{26}$$

It is to be noted that Eq. 23-26 can be easily solved using the symbolic MATLAB software for $m \ge 1$. The general solution for Eq. 23 in terms of particular solutions i.e., $f_m^\star(\eta)$, $\theta_m^\star(\eta)$ and $\phi_m^\star(\eta)$ are given in the following forms

$$\begin{cases} f_m(\eta) = f_m^\star(\eta) + c_1 + c_2 \exp(\eta) + c_3 \exp(-\eta), \\ \theta_m(\eta) = \theta_m^\star(\eta) + c_4 \exp(\eta) + c_5 \exp(-\eta), \\ \phi_m(\eta) = \phi_m^\star(\eta) + c_6 \exp(\eta) + c_7 \exp(-\eta), \end{cases} \tag{27}$$

where,

$$c_2 = c_4 = c_6 = 0, c_3 = \frac{\partial f_m^\star(0)}{\partial \eta}, c_1 = -c_3 - f_m^\star(0), c_5 = -\theta_m^\star(0), c_7 = -\phi_m^\star(0). \tag{28}$$

As stated by Liao [37-40], convergence of the HAM-series solutions largely depends on the values of auxiliary parameters. Hence, the optimal values of h_f, h_θ and h_ϕ can be found by minimizing the square residual errors as follows [40]

$$\begin{cases} \boldsymbol{\epsilon}_f^m(h_f) = \frac{1}{q+1} \sum_{i=0}^{q} \left[\mathbf{N}_f \left(\sum_{j=0}^{m} f(\eta) \right)_{\eta = i\delta\eta} \right]^2 d\eta, \\ \boldsymbol{\epsilon}_\theta^m(h_\theta) = \frac{1}{q+1} \sum_{i=0}^{q} \left[\mathbf{N}_\theta \left(\sum_{j=0}^{m} f(\eta), \sum_{j=0}^{m} \theta(\eta), \sum_{j=0}^{m} \phi(\eta) \right)_{\eta = i\delta\eta} \right]^2 d\eta, \\ \boldsymbol{\epsilon}_\phi^m(h_\phi) = \frac{1}{q+1} \sum_{i=0}^{q} \left[\mathbf{N}_\phi \left(\sum_{j=0}^{m} f(\eta), \sum_{j=0}^{m} \theta(\eta), \sum_{j=0}^{m} \phi(\eta) \right)_{\eta = i\delta\eta} \right]^2 d\eta, \end{cases} \tag{29}$$

and,

$$h_f : \lim_{m\to\infty} \epsilon_f^m(h_f) = 0, h_\theta : \lim_{m\to\infty} \epsilon_\theta^m(h_\theta) = 0, h_\phi : \lim_{m\to\infty} \epsilon_\phi^m(h_\phi) = 0, \quad (30)$$

where $q = 20$ and $\delta\eta = 0.5$. In this regard, Table 1 tabulates the optimal values of auxiliary parameters and corresponding square residual errors for different orders of approximation in terms of $\lambda = 0.4$, $\mathrm{Ha} = 1$, $\psi = 45°$, $\mathrm{Pr} = 1$, $\mathrm{Nb} = \mathrm{Nt} = 0.5$, $\mathrm{Nr} = 0.3$, $\mathrm{Ec} = 0.2$ and $\mathrm{Le} = 1$. From this table, it can be seen that $h_f = -0.7083$, $h_\theta = -0.8958$ and $h_\phi = -0.6736$ will hereafter be employed within the text.

To summarize, the HAM algorithm can be provided as follows

a) Set $m = 1$.
b) Substitute Eq. 12 into Eq. 26 and obtain $\mathbf{R}_1^f(\eta)$, $\mathbf{R}_1^\theta(\eta)$ and $\mathbf{R}_1^\phi(\eta)$.
c) Substitute $\mathbf{R}_1^f(\eta)$, $\mathbf{R}_1^\theta(\eta)$ and $\mathbf{R}_1^\phi(\eta)$ into Eq. 23.
d) Compute $c_1, c_2, \ldots, c_7$ for $m \geq 1$ and obtain $f_1(\eta)$, $\theta_1(\eta)$ and $\phi_1(\eta)$.
e) Substitute $f_1(\eta)$, $\theta_1(\eta)$ and $\phi_1(\eta)$ into Eq. 26 and obtain $\mathbf{R}_2^f(\eta)$, $\mathbf{R}_2^\theta(\eta)$ and $\mathbf{R}_2^\phi(\eta)$.
f) Repeat steps 2-4 m times.
g) Obtain $f_M(\eta)$, $\theta_M(\eta)$ and $\phi_M(\eta)$ where M is the number of iterations.
h) Check for convergence of the computations.

Table 1
Selection of auxiliary parameters

m	h_f	ϵ_f^m	h_θ	ϵ_θ^m	h_ϕ	ϵ_ϕ^m
2	-0.6402	3.48×10^{-5}	-0.8214	7.29×10^{-6}	-0.5552	5.33×10^{-5}
5	-0.6746	7.16×10^{-6}	-0.8690	8.10×10^{-7}	-0.6140	1.60×10^{-5}
10	-0.6940	2.96×10^{-7}	-0.8841	1.90×10^{-7}	-0.6470	8.09×10^{-6}
15	-0.7016	8.18×10^{-8}	-0.8907	4.98×10^{-8}	-0.6615	1.15×10^{-6}
20	-0.7083	4.53×10^{-9}	-0.8958	5.91×10^{-9}	-0.6736	8.54×10^{-7}

3.2 RKF45M

The generated RKF45M algorithm in MAPLE 13 worksheet together with the shooting technique, as it is illustrated in Figure 1, converts Eq. 7 to a set of initial value problems with the convergence criterion 10^{-6}, step size $\Delta\eta = 0.01$ and upper bound of the integral $\eta_\infty = 10$. For more details on the RKF45M, see Refs. [7,41].

4. Results and Discussion

In this section, the obtained results from evaluating the flow of Casson fluid above a moving flat plate with viscous dissipation, magnetic force, radiation effects and convective boundary conditions is reported based on the Buongiorno's mathematical model. In order to ensure the accuracy and effectiveness of the present analytical and numerical solutions, the obtained results are compared with those available findings in the literatures in subsection 1. Then, further details about this paper are available in subsection 2.

```
> restart
> with(plot)
> macro(x = eta):
> fixedparameters := einf := 10: lambda := 0.4: Ha := 1: psi := 45: Pr := 1: Nb := 0.5:
Nt := 0.5: Nr := 0.3 :Ec := 0.2 :Le := 1:
> eqs1:= (1 + (1/lambda)) * diff(f(eta), eta, eta, eta) + f(eta) * diff(f(eta), eta, eta)
-diff(f(eta), eta) * (diff(f(eta), eta)+(Ha)^2 * (sin(psi))^2) = 0:
> eqs2:= (1/Pr) * diff(theta(eta), eta, eta) + (1/2) * f(eta) * diff(theta(eta), eta)
+Nb * diff(phi(eta), eta) * diff(theta(eta), eta) + Nt * diff(theta(eta), eta)
* diff(theta(eta), eta) + (1/2) * Nr * f(eta) * diff(theta(eta), eta) + Ec * (1 + (1/lambda))
* diff(f(eta), eta, eta) * diff(f(eta), eta, eta):
> eqs3:= diff(phi(eta), eta, eta) + (1/2) * Le * f(eta) * diff(phi(eta), eta) + (Nt/Nb)
* diff(theta(eta), eta, eta):
> bcs1 := f(0) = 0, (D(f))(0) = 1, theta(0) = 1, phi(0) = 1:
> bcs2 := (D(f))(einf) = 0, theta(einf) = 0, phi(einf) = 0:
eqs := {eqs1, eqs2, eqs3, bcs1, bcs2,}:
> Q := dsolve(eqs, {f(x), theta(x), phi(x)}, numeric, output = listprocedure):
> F := eval(f(x), Q); D1F := eval(diff(f(x), x), Q); D2F := eval(diff(f(x), x, x), Q):
> THETA := eval(theta(x), Q); D1THETA := eval(diff(theta(x), x), Q):
> PHI := eval(phi(x), Q); D1PHI := eval(diff(phi(x), x), Q):
> plot([F(X), D1F(x), D2F(x)], x = 0..einf):
> p1 := plot(D1F(x), x = 0..einf):
> p2 := plot(THETA(x), x = 0..einf):
> p3 := plot(PHI(x), x = 0..einf):
> evalf({D2F(0), -D1THETA(0), -D1PHI(0)}):
> Cf := (1 + (1/lambda)) * D2F(0):
> Nux := -D1THETA(0):
> Shx := -D1PHI(0):
```

Fig. 1. Generated RKF45M algorithm in MAPLE 13 worksheet together with the shooting technique

4.1 Comparison and Validation

Example 1. This example aims to provide a comparison between the present solutions and those reported in Refs. [42,43] to determine the values of $\left(\frac{\partial^2 f}{\partial \eta^2}\right)_{\eta=0}$ in terms of λ. Haldar *et al.,* [42], suggest flow of the Casson fluid past a power-law stretching surface is investigated numerically using the RK4M together with the Newton's technique while Bhattacharyya *et al.,* [43] suggests a closed-form solution for the flow of Casson fluid past a porous shrinking / stretching surface. It is to be mentioned here that the other pertinent parameters dealt with this paper are set to zero i.e., $\mathrm{Ha} = \psi = \mathrm{Pr} = \mathrm{Nb} = \mathrm{Nt} = \mathrm{Nr} = \mathrm{Ec} = \mathrm{Le} = 0$. From Table 2, it is seen that the values of $\left(\frac{\partial^2 f}{\partial \eta^2}\right)_{\eta=0}$ decrease with an increase in λ for all cases listed in this table. Moreover, since the maximum relative error between the HAM / RKF45M and those of Refs. [42,43] does not exceed 0.008% / 0.035% and 0.009% / 0.037%, respectively, the validity of the present solutions is confirmed.

Example 2. At this point, MHD three-dimensional flow of a fluid past a linearly stretching surface which is provided in Chamkha research [44], is compared with the present solutions to calculate the values of $\left(\frac{\partial^2 f}{\partial \eta^2}\right)_{\eta=0}$ in terms of Ha. The pertinent parameters in this case are provided as follows, $\lambda \to \infty$, $\mathrm{Pr} = 6.7$ and $\psi = \mathrm{Nb} = \mathrm{Nt} = \mathrm{Nr} = \mathrm{Ec} = \mathrm{Le} = 0$. Furthermore, the obtained results correspond to this example are rounded up to five digits. As it is shown in Table 3, the values

of $\left(\frac{\partial^2 f}{\partial \eta^2}\right)_{\eta=0}$ decrease with an increase in Ha. The results of HAM / RKF45M and Chamkha [44] only suffer from a relative error of at most 0.031% / 0.033%. Hence, it can be emphasized that the present solutions are consistent with the findings of Chamkha [44]. However, there is a minor difference between these results which is largely due to the different solution methodologies.

Table 2

Values of $\left(\frac{\partial^2 f}{\partial \eta^2}\right)_{\eta=0}$ compared with Refs. [42,43] for $\mathrm{Ha} = \psi = \mathrm{Pr} = \mathrm{Nb} = \mathrm{Nt} = \mathrm{Nr} = \mathrm{Ec} = \mathrm{Le} = 0$

λ	Present solution-HAM	Present solution-RKF45M	Ref. [42]	Ref. [43]
0.5	-0.577398	-0.577405	-0.577351	-0.577865
1	-0.707186	-0.707194	-0.707107	-0.707243
2	-0.816529	-0.816538	-0.816497	-
5	-0.912963	-0.912970	-0.912871	-0.913120

Table 3

Values of $\left(\frac{\partial^2 f}{\partial \eta^2}\right)_{\eta=0}$ compared with Chamkha [44] for $\lambda \to \infty$, $\mathrm{Pr} = 6.7$ and $\psi = \mathrm{Nb} = \mathrm{Nt} = \mathrm{Nr} = \mathrm{Ec} = \mathrm{Le} = 0$

Ha	0	1	2	3	4
Present solution-HAM	-1.00114	-1.41544	-2.23690	-3.16297	-5.09921
Present solution-RKF45M	-1.00116	-1.41546	-2.23690	-3.16297	-5.09921
Ref. [44]	-1.00180	-1.41602	-2.23731	-3.16351	-5.10068

Example 3. This example illustrates a comparison between the present solutions and Abdul Hakeem *et al.,*[45] to determine the values of $\left(\frac{\partial^2 f}{\partial \eta^2}\right)_{\eta=0}$ in terms of ψ considering $\lambda = 0.4$, $\mathrm{Ha} = 1$ and $\mathrm{Pr} = \mathrm{Nb} = \mathrm{Nt} = \mathrm{Nr} = \mathrm{Ec} = \mathrm{Le} = 0$. In Ref. [45], the flow of Casson fluid with thermal radiation and velocity slip boundary conditions is investigated using the RK4M together with the shooting technique. Based on the results of Table 4, the values of $\left(\frac{\partial^2 f}{\partial \eta^2}\right)_{\eta=0}$ decrease with an increase in ψ. The difference in these findings is due to a maximum relative error equals to 1.082% / 0.377% between the HAM / RKF45M and Abdul Hakem *et al.,* [45] which can verify the present solutions.

Table 4

Values of $\left(\frac{\partial^2 f}{\partial \eta^2}\right)_{\eta=0}$ compared with Abdul Hakeem *et al.,* [45] for $\lambda = 0.4$, $\mathrm{Ha} = 1$ and $\mathrm{Pr} = \mathrm{Nb} = \mathrm{Nt} = \mathrm{Nr} = \mathrm{Ec} = \mathrm{Le} = 0$

ψ	0°	30°	45°	60°
Present solution-HAM	-1.0612	-1.1681	-1.2547	-1.3399
Present solution-RKF45M	-1.0747	-1.1712	-1.2604	-1.3442
Ref. [45]	-1.0797	-1.1763	-1.2644	-1.3482

Example 4. The final stage is to compare the values of $\left(\frac{\partial \theta}{\partial \eta}\right)_{\eta=0}$ in terms of Pr obtained by the present solutions with those reported in Gorla and Sidawi [46]. The numerical procedure for solving two-point BVPs is utilized to investigate the effect of mass transfer rate on the vertical stretching surface.[46] The results of this example are provided with $\lambda \to \infty$ and $\mathrm{Ha} = \psi = \mathrm{Nb} = \mathrm{Nt} = \mathrm{Nr} =$

$\mathrm{Ec} = \mathrm{Le} = 0$. From Table 5, it is observed that the values of $\left(\frac{\partial\theta}{\partial\eta}\right)_{\eta=0}$ increases with a decrease in Pr. Above all, the relative error between the HAM / RKF45M and Gorla and Sidawi [46] does not exceed 0.129% / 0.153%; accordingly, the present solutions are in agreement with Gorla and Sidawi [46].

Table 5
Values of $\left(\frac{\partial\theta}{\partial\eta}\right)_{\eta=0}$ compared with Gorla and Sidawi [46] for $\lambda \to \infty$ and $\mathrm{Ha} = \psi = \mathrm{Nb} = \mathrm{Nt} = \mathrm{Nr} = \mathrm{Ec} = \mathrm{Le} = 0$

Pr	0.7	3	7	10
Present solution-HAM	-0.45416	-1.16608	-1.89578	-2.30312
Present solution-RKF45M	-0.45399	-1.16573	-1.89546	-2.30288
Ref. [46]	-0.45593	-1.16669	-1.89691	-2.30350

4.2 Further Details

In this subsection, unless stated otherwise, the pertinent parameters are provided as follows, $\lambda = 0.4$, $\mathrm{Ha} = 1$, $\psi = 45°$, $\mathrm{Pr} = 1$, $\mathrm{Nb} = \mathrm{Nt} = 0.5$, $\mathrm{Nr} = 0.3$, $\mathrm{Ec} = 0.2$ and $\mathrm{Le} = 1$.

Figure 2 shows variation in the local Nusselt number with λ and Ha. The obtained results correspond to this figure demonstrate that the local Nusselt number decreases with an increase in λ. This is because, an increase in λ decreases the yield stress of the fluid that leads eventually to an increase in the plastic dynamic viscosity as well as its viscous forces on the flow. Indeed, one can imagine the flow of Casson fluid to act as a solid until a yield stress is exceeded [47]. Moreover, as it is seen from Figure 2, the local Nusselt number decreases with an increase in Ha by reason of a drag-like force, namely Lorentz force. This force tends to resist flow of the fluid and consequently retards its motion. In addition, presence of the thermal radiation might well lead to a decrease in the local Nusselt number [45]. The point is, an increase in thermal radiation leads to generate the internal heat energy.

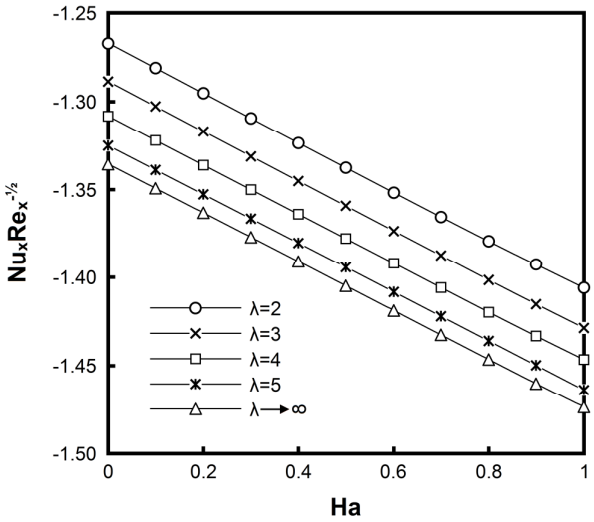

Fig. 2. HAM-series solution for the values of $\mathrm{Nu}_x\mathrm{Re}_x^{-\frac{1}{2}}$-Ha curve in terms of λ

As Figure 3 depicts, for thermophoresis parameter less than 0.3, the local Nusselt number increases with an increase in Pr. It is due to the fact that, the higher value of Pr has the convection coefficient larger than its conduction coefficient. Furthermore, one can observe that the thermal boundary layer thickens with an increase in Pr. For thermophoresis parameter equal to 0.3, there exists no considerable difference between these configurations, and the corresponding value of the local Nusselt number is approximately -0.681. It can be proved that the thermophoretic force plays an important role in the motion of nanoparticles from the hot flat plate to the quiescent fluid. However, for thermophoresis parameter more than 0.3, the local Nusselt number decreases with an increase in Pr.

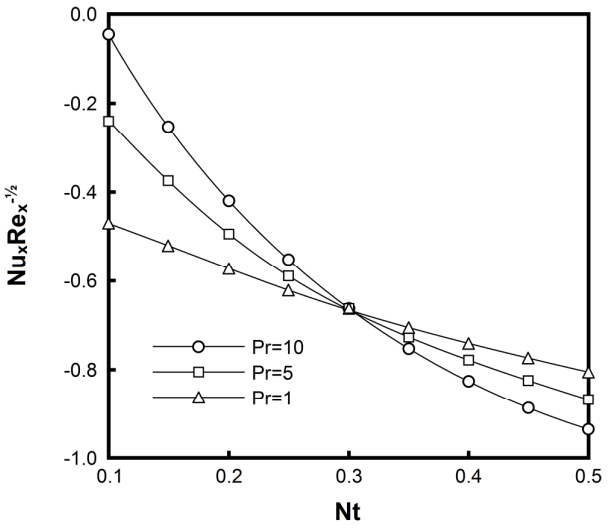

Fig. 3. HAM-series solution for the values of $\mathrm{Nu}_x\mathrm{Re}_x^{-\frac{1}{2}}$-$\mathrm{Nt}$ curve in terms of Pr

The effect of viscous dissipation parameter i.e., Eckert number on variation in the local Nusselt number is illustrated in Figure 4**.** From this figure, it is seen that the local Nusselt number decreases with an increase in Ec. This is because, an increase in Ec increases the thermal diffusion which is led to an increase in the thermal conductivity of the flow. Furthermore, accounting for $\mathrm{Ec} > 0$ provides cooling of the flat plate [48,49] so that the generated thermal energy will be stored in the vicinity of the fluid. Hence, the thermal boundary layer thickens with an increase in dissipation. Figure 4 also emphasizes that the local Nusselt number increases with an increase in Nr. This is because, an increase in Nr increases the Rosseland absorptivity parameter i.e., β_R which is led to a decrease in divergence of the radiation heat flux i.e., $\frac{\partial q_r}{\partial y}$.

As Figure 5 depicts, the nanoparticle concentration boundary layer thickens with an increase in the mass diffusion. Since $\mathrm{Le} > 1$ the heat diffuses through flat plate more rapidly than the nanoparticles [50]. However, in case of $\mathrm{Le} = 1$ the heat and nanoparticles diffuse at the same rate. Figure 5 also emphasizes that the nanoparticle concentration boundary layer thickens with an increase in Nt which is due to the formation of a nanoparticle free layer in the vicinity of the flat plate.

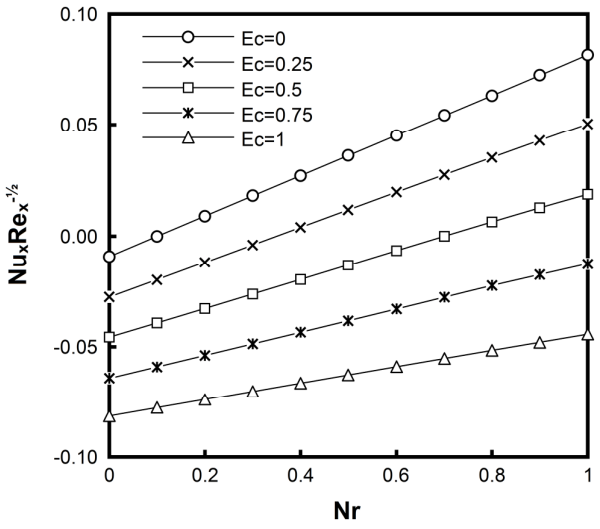

Fig. 4. HAM-series solution for the values of $\mathrm{Nu}_x\mathrm{Re}_x^{-\frac{1}{2}}$-Nr curve in terms of Ec

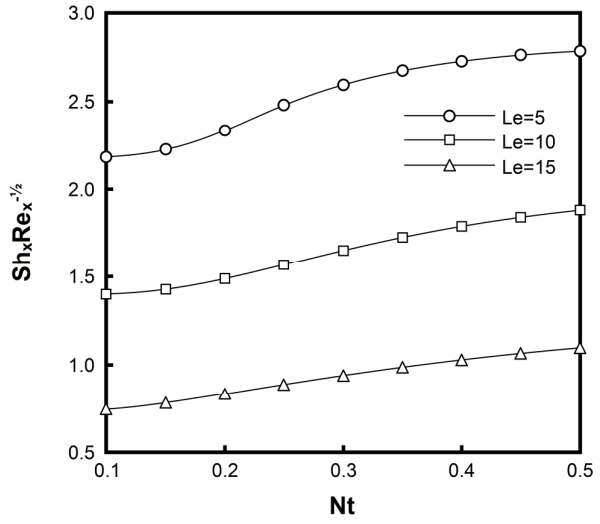

Fig. 5. HAM-series solution for the values of $\mathrm{Sh}_x\mathrm{Re}_x^{-\frac{1}{2}}$-Nt curve in terms of Le

Figure 6 shows that the local Sherwood number is a decreasing function of Nb. This is because, an increase in Nb results in an interaction between the fluid and nanoparticles that leads eventually to a decrease in the nanoparticle concentration boundary layer thickness.

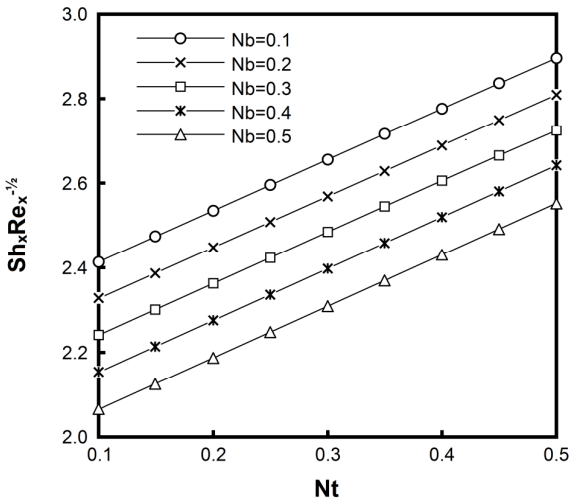

Fig. 6. HAM-series solution for the values of $\mathrm{Sh}_x\mathrm{Re}_x^{-\frac{1}{2}}$-Nt curve in terms of Nb

5. Concluding Remarks

The objective of this paper was to introduce the analytical and numerical solutions i.e., HAM and RKF45M to study 2D Sakiadis flow of Casson fluid with cross diffusion, inclined magnetic force, viscous dissipation and thermal radiation. To this end, the set of governing partial differential equations were converted to the nonlinear ordinary differential equations based on Buongiorno's mathematical model. The present solutions were compared and validated by those available results in the literatures. The main results that can be inferred from this paper are reported as follows

a) Accounting for the effect of Lorentz force leads to resist flow of the fluid.
b) The internal heat energy is generated by an increase in the thermal radiation. Therefore, this increment leads to a decrease in the local Nusselt number.
c) The effect of thermophoretic force on the local Nusselt number can be usually ignored for thermophoresis parameter equals to 0.3.
d) The thermal boundary layer thickness increases with an increase in the dissipation due to the generation of thermal energy in the vicinity of the fluid.
e) The local Sherwood number inversely depends on the mass diffusion.

References

[1] Sakiadis, Byron C. "Boundary-layer behavior on continuous solid surfaces: I. Boundary-layer equations for two-dimensional and axisymmetric flow." *AIChE Journal* 7, no. 1 (1961): 26-28.
[2] Sakiadis, B. C. "Boundary-layer behavior on continuous solid surfaces: II. The boundary layer on a continuous flat surface." *AIChE Journal* 7, no. 2 (1961): 221-225.
[3] Blasius, Heinrich. "Grenzschichten in Flüssigkeiten mit kleiner Reibung" *Z. Math. Phys*. 56 (1908) 1-37.
[4] C. Sulochana, G.P. Ashwinkumar, N. Sandeep. "Joule heating effect on a continuously moving thin needle in MHD Sakiadis flow with thermophoresis and Brownian moment", *Eur. Phys. J. Plus* 132 no. 9, (2017) 1-14.
[5] Soid, Siti Khuzaimah, Anuar Ishak, and Ioan Pop. "Boundary layer flow past a continuously moving thin needle in a nanofluid." *Applied Thermal Engineering* 114 (2017): 58-64..
[6] Bataller, Rafael Cortell. "Radiation effects for the Blasius and Sakiadis flows with a convective surface boundary condition." *Applied Mathematics and Computation* 206, no. 2 (2008): 832-840.
[7] Aziz, Abdul. "A similarity solution for laminar thermal boundary layer over a flat plate with a convective surface boundary condition." *Communications in Nonlinear Science and Numerical Simulation* 14, no. 4 (2009): 1064-1068.

[8] T. Hayat, Z. Iqbal, M. Qasim, S. Obaidat. "Steady flow of an Eyring Powell fluid over a moving surface with convective boundary conditions*", Int. J. Heat Mass Transf.* 55 no. 7-8, (2012): 1817-1822.
[9] Bachok, Norfifah, Anuar Ishak, and Ioan Pop. "Flow and heat transfer characteristics on a moving plate in a nanofluid." *International Journal of Heat and Mass Transfer* 55, no. 4 (2012): 642-648.
[10] Ahmad, Syakila, Azizah Mohd Rohni, and Ioan Pop. "Blasius and Sakiadis problems in nanofluids." *Acta Mechanica* 218, no. 3-4 (2011): 195-204.
[11] Ishak, Anuar, Roslinda Nazar, and Ioan Pop. "Flow and heat transfer characteristics on a moving flat plate in a parallel stream with constant surface heat flux." *Heat and mass transfer* 45, no. 5 (2009): 563-567.
[12] Pantokratoras, Asterios. "Non-similar Blasius and Sakiadis flow of a non-Newtonian Carreau fluid." *Journal of the Taiwan Institute of Chemical Engineers* 56 (2015): 1-5.
[13] Rao, M. Anandha. "Measurement of flow and viscoelastic properties." In *Rheology of Fluid and Semisolid Foods*, pp. 59-151. Springer, Boston, MA, 2007.
[14] T. Hayat, Z. Iqbal, M. Mustafa, A. Alsaedi. "Momentum and heat transfer of an upper-converted Maxwell fluid over a moving surface with convective boundary conditions", *Nucl. Eng. Des*. 252, (2012): 242-247.
[15] Girgin, Zekeriya. "Solution of the Blasius and Sakiadis equation by generalized iterative differential quadrature method." *International Journal for Numerical Methods in Biomedical Engineering* 27, no. 8 (2011): 1225-1234.
[16] Arikoglu, Aytac, and Ibrahim Ozkol. "Inner-outer matching solution of Blasius equation by DTM." *Aircraft Engineering and Aerospace Technology* 77, no. 4 (2005): 298-301.
[17] Andersson, Helge I., and Jan B. Aarseth. "Sakiadis flow with variable fluid properties revisited." *International journal of engineering science* 45, no. 2-8 (2007): 554-561.
[18] Xu, Ding, and Xin Guo. "Application of fixed point method to obtain semi-analytical solution to Blasius flow and its variation." *Applied Mathematics and Computation* 224 (2013): 791-802.
[19] Fazio, Riccardo. "The iterative transformation method for the Sakiadis problem." *Computers & Fluids* 106 (2015): 196-200.
[20] Fazio, R. "The Blasius problem formulated as a free boundary value problem." *Acta mechanica* 95, no. 1-4 (1992): 1-7.
[21] Ghiasi, Emran Khoshrouye, and Reza Saleh. "Non-dimensional optimization of magnetohydrodynamic Falkner-Skan fluid flow", *INAE Lett.* 3 no. 3, (2018): 143-147.
[22] Khoshrouye Ghiasi, Emran, and Reza Saleh. "2D flow of Casson fluid with non-uniform heat source/sink and Joule heating", *Front. Heat Mass Transf*. 12, (2019): 1-7.
[23] R. Rana, R. Mehmood, PV.S. Narayana, N.S. Akbar. "Free convection nonaligned non-Newtonian flow with non-linear thermal radiation", *Commun. Theor. Phys.* 66 no. 6, (2016): 687-693.
[24] Rana, S., Rashid Mehmood, and Noreen Sher Akbar. "Mixed convective oblique flow of a Casson fluid with partial slip, internal heating and homogeneous–heterogeneous reactions." *Journal of Molecular liquids* 222 (2016): 1010-1019.
[25] Z. Iqbal, R. Mehmood, E. Azhar, Z. Mehmood. "Impact of inclined magnetic field on micropolar Casson fluid using Keller box algorithm", *Eur. Phys. J. Plus*, 132 no. 4, (2017): 1-13.
[26] Z. Mehmood, R. Mehmood, Z. Iqbal. "Numerical investigation of micropolar Casson fluid over a stretching sheet with internal heating", *Commun. Theor. Phys.* 67 no. 4, (2016): 443-448.
[27] R. Mehmood, S. Rana, N. Maraj. "Transverse transport of polymeric nanofluid under pure internal heating: Keller box algorithm", *Commun. Theor. Phys*. 70 no. 1, (2017): 106-118.
[28] R. Mehmood, S. Rana. "Thermal transport of rate-type fluid impinging obliquely over a heated sheet", *Pramana* 91 no. 5, (2018): 71-79.
[29] Mehmood, Rashid, S. Nadeem, S. Saleem, and Noreen Sher Akbar. "Flow and heat transfer analysis of Jeffery nano fluid impinging obliquely over a stretched plate." *Journal of the Taiwan Institute of Chemical Engineers* 74 (2017): 49-58.
[30] Ghiasi, Emran Khoshrouye, and Reza Saleh. "Constructing analytic solutions on the Tricomi equation." *Open Physics* 16, no. 1 (2018): 143-148.
[31] Buongiorno, Jacopo. "Convective transport in nanofluids." *Journal of heat transfer* 128, no. 3 (2006): 240-250.
[32] M. Ghassemi, A. Shahidian. "Nano and bio heat transfer and fluid flow", *Elsevier Inc., San Diego, USA,* 2017.
[33] A. Ostadfar. "Biofluid mechanics: Principles and applications", *Elsevier Inc., London, UK,* 2016.
[34] P.M. Doran. "Bioprocess engineering principles", *2nd ed., Elsevier Inc., Waltham, USA,* 2013.
[35] N. Casson. "Rheology of disperse systems", *C.C. Mill., London, UK,* 1959.
[36] S. Rosseland, Astrophysik und atom-theoretische Grundlagen, Springer-Verlag, Berlin, Germany, 1931.
[37] S.J. Liao. "The proposed homotopy analysis technique for the solution of nonlinear problems", PhD thesis, Shanghai Jiao Tong Univ., 1992.

[38] S.J. Liao, "Beyond Perturbation: Introduction to the homotopy analysis method", *Chapman & Hall/CRC Press*, Boca Raton, USA, 2003.
[39] Liao, Shijun. "On the homotopy analysis method for nonlinear problems." *Applied Mathematics and Computation* 147, no. 2 (2004): 499-513.
[40] Liao, Shijun. "An optimal homotopy-analysis approach for strongly nonlinear differential equations." *Communications in Nonlinear Science and Numerical Simulation* 15, no. 8 (2010): 2003-2016.
[41] Rauf, A., M. K. Siddiq, F. M. Abbasi, M. A. Meraj, M. Ashraf, and S. A. Shehzad. "Influence of convective conditions on three dimensional mixed convective hydromagnetic boundary layer flow of Casson nanofluid." *Journal of Magnetism and Magnetic Materials* 416 (2016): 200-207.
[42] S. Haldar, S. Mukhopadhyay, G.C. Layek. "Dual solutions of Casson fluid flows over a power-law stretching sheet", *J. Appl. Mech. Tech. Phys.* 58 no. 4, (2017): 629-634.
[43] Bhattacharyya, Krishnendu, Tasawar Hayat, and Ahmed Alsaedi. "Exact solution for boundary layer flow of Casson fluid over a permeable stretching/shrinking sheet." *ZAMM-Journal of Applied Mathematics and Mechanics/Zeitschrift für Angewandte Mathematik und Mechanik* 94, no. 6 (2014): 522-528.
[44] Chamkha, Ali J. "Hydromagnetic three-dimensional free convection on a vertical stretching surface with heat generation or absorption." *International journal of heat and fluid flow* 20, no. 1 (1999): 84-92.
[45] A.K. Abdul Hakeem, P. Renuka, N. Vishnu Ganesh, R. Kalaivanan, B. Ganga. "Influence of inclined Lorentz forces on boundary layer flow of Casson fluid over an impermeable stretching sheet with heat transfer", *J. Magn. Magn. Mater.* 401, (2016): 354-361.
[46] Gorla, Rama Subba Reddy, and Ibrahim Sidawi. "Free convection on a vertical stretching surface with suction and blowing." *Applied Scientific Research* 52, no. 3 (1994): 247-257.
[47] Ghiasi, Emran Khoshrouye, and Reza Saleh. "Unsteady shrinking embedded horizontal sheet subjected to inclined Lorentz force and Joule heating, an analytical solution." *Results in Physics* 11 (2018): 65-71.
[48] B. Lakshminarayana. "Fluid dynamics and heat transfer of turbomachinery", *John Wiley & Sons Inc.*, New York, USA, 1996.
[49] M. Abd El-Aziz. "Temperature dependent viscosity and thermal conductivity effects on combined heat and mass transfer in MHD three-dimensional flow over a stretching surface with Ohmic heating", *Meccanica* 42 (2007): 375-386.
[50] E. Khoshrouye Ghiasi, R. Saleh. "Nonlinear stability and thermomechanical analysis of hydromagnetic Falkner-Skan Casson conjugate fluid flow over an angular-geometric surface based on Buongiorno's model using homotopy analysis method and its extension", *Pramana* 92 no. 1 (2019): 1-12.